

# Amplification and oscillations in the FAK/Src kinase system during integrin signaling

G. Caron-Lormier<sup>1</sup>, H. Berry\*

*Equipe de Recherche sur les Relations Matrice Extracellulaire-Cellules (ERRMECe), Université de Cergy-Pontoise, 2 avenue A. Chauvin, B.P. 222, 95302 Cergy Pontoise Cedex, France*

Received 27 May 2003; received in revised form 11 June 2004; accepted 9 August 2004  
Available online 25 September 2004

## Abstract

Integrin signaling is a major pathway of cell adhesion to extracellular matrices that regulates many physiological cell behaviors such as cell proliferation, migration or differentiation and is implied in pathologies such as tumor invasion. In this paper, we focused on the molecular system formed by the two kinases FAK (focal adhesion kinase) and Src, which undergo auto- and co-activation during early steps of integrin signaling. The system is modelled using classical kinetic equations and yields a set of three nonlinear ordinary differential equations describing the dynamics of the different phosphorylation forms of FAK. Analytical and numerical analysis of these equations show that this system may in certain cases amplify incoming signals from the integrins. A quantitative condition is obtained, which indicates that the total FAK charge in the system acts as a critical mass that must be exceeded for amplification to be effective. Furthermore, we show that when FAK activity is lower than Src activity, spontaneous oscillations of FAK phosphorylation forms may appear. The oscillatory behavior is studied using bifurcation and stability diagrams. We finally discuss the significance of this behavior with respect to recent experimental results evidencing FAK dynamics.

© 2004 Elsevier Ltd. All rights reserved.

*Keywords:* Integrin signaling; Focal adhesion kinase; Src

## 1. Introduction

Cell adhesion to the extracellular matrix (ECM) is a crucial regulator of many physiological cell functions in multicellular organisms, including cell cycle, survival, proliferation, differentiation or migration (Damsky and Ilic, 2002; Martin et al., 2002), and is thus implied in several pathologies, such as tumor invasion (Crowe and Shuler, 1999; Ruoslahti, 1999). These effects are mediated by a few classes of receptor (Hynes, 1999), among which the integrin family plays a predominant role (Schwartz, 2001). Integrins are transmembrane

heterodimeric receptors that specifically recognize and bind to ligands of the ECM (Hynes, 1999). Although devoid of an intrinsic enzymatic activity, the cytoplasmic domains of ECM-bound integrins trigger the recruitment of a large number of cytoplasmic, cytoskeletal and transmembrane proteins into discrete regions on the cytoplasmic side of the plasma membrane, referred to as focal adhesions (FAs) (Katz et al., 2000; Cukierman et al., 2001). FAs are structural anchorage sites for attachment to the ECM and represent a continuous physical link between the ECM and the intracellular actin cytoskeleton. But they also are functional complexes which initiate multiple signaling pathways inside the cell, that ultimately lead to the aforementioned traits or activities (outside-in signaling). Examples of proteins recruited at FAs include  $\alpha$ -actinin, talin, paxilin, phosphatidylinositol 3-kinase (PI3-K) or the adaptor protein Grb-2 (LaFlamme and Auer, 1996).

\*Corresponding author. Tel.: 33-1-34-25-66-71; fax: 33-1-34-25-65-52.

*E-mail addresses:* [geoffrey.caron-lormier@univ-rennes1.fr](mailto:geoffrey.caron-lormier@univ-rennes1.fr) (G. Caron-Lormier), [hugues.berry@bio.u-cergy.fr](mailto:hugues.berry@bio.u-cergy.fr) (H. Berry).

<sup>1</sup>Present address: UMR 6552 E.V.E: Ethologie-eVolution-Ecologie, Avenue du General Leclerc, Campus BEAULIEU, Bât. 25, 35042 RENNES Cedex, France.

The cytosolic protein tyrosine kinases (PTKs), FAK (focal adhesion kinase) and Src are early (proximal) mediators of integrin signaling. They seem essential for multicellular life, as FAK-null mice die early during embryogenesis (Ilic et al., 1995). Accordingly, FAK signaling has been directly or indirectly implicated in many cell biological traits, including cell adhesion (Vuori et al., 1996), spreading (Owen et al., 1999; Wennerberg et al., 2000), proliferation and cycle (Reiske et al., 2000), migration (Reiske et al., 1999; Wang et al., 2001), apoptosis (anoikis) (Cary and Guan, 1999; Schaller, 2001) or tumor invasion (Owens et al., 1995; Slack et al., 2001).

Upon integrin binding to the ECM, FAK localizes to the FAs (Schaller et al., 1992) where it may undergo phosphorylation at multiple sites. The mechanism by which FAK is targeted to the FA is still unclear, although observations suggest that it might be mediated by FAK binding to the cytoskeletal proteins talin and/or paxillin (Schaller, 2001). FAK phosphorylation after recruitment into FAs regulates its enzyme activity as well as its ability to bind and/or activate other signaling molecules. A major FAK phosphorylation site is tyrosine 397. This autophosphorylation site becomes, once phosphorylated, a docking site for the SH2 domains of a number of signaling proteins, including Src, PI3-K and Grb7 (Chen and Guan, 1994; Reiske et al., 1999). Once recruited to the FAs via pY397FAK, PI3-K and Grb7 trigger signaling pathways that control cell motility (Cary and Guan, 1999) or growth (Danen and Yamada, 2001). Binding of the PTK Src to pY397FAK is another critical point of integrin-mediated signaling. The formation of this molecular complex activates Src (Pawson et al., 2001), which, in turn, phosphorylates other proteins such as the docking protein p130<sup>Cas</sup> (Vuori et al., 1996; Cary et al., 1998). Phosphorylated p130<sup>Cas</sup> itself can bind the adaptor protein Crk, that has been shown to regulate cell migration (Klemke et al., 1998; Cary and Guan, 1999) and proliferation (Bouton et al., 2001). Active Src has furthermore been evidenced to phosphorylate FAK on tyrosines 925, 576 and 577. FAK Y925 phosphorylation creates a binding site for the adaptor protein Grb2 that recruits the protein SOS. The Grb2/SOS complex is itself an activator of the Ras and MAP kinase pathways that regulate cell proliferation (Schlaepfer and Hunter, 1997; Schlaepfer et al., 1998). FAK tyrosines 576 and 577 are located in its activation loops, so that their phosphorylation by Src yields the active enzymatic form of FAK. Active FAK can then transmit downstream signals, as well as phosphorylate the tyrosine 397 (hence the autophosphorylation site) of other FAK molecules.

Recently, a plausible sequential scheme for FAK and Src interactions has emerged (Thomas and Brugge, 1997; Schaller, 2001). According to this scheme, integrin–ligand binding triggers FAK recruitment to

the FAs and its phosphorylation on tyrosine 397 by active FAK (autoactivation). The resulting pY397FAK presents a high affinity binding site for Src (Pawson et al., 2001). The process of Src binding via its SH2 domain requires a conformational change in Src that stabilizes it into its fully active form (Schaller et al., 1999; Young et al., 2001). Active Src remains bounded to pY397FAK and further phosphorylates FAK on tyrosines 576 and 577 (Chaudhary et al., 2002), yielding the active form of FAK, that, in turn catalyses FAK phosphorylation on Y397 (Owen et al., 1999; Ruest et al., 2000). This mechanism thus implies both indirect autoactivation (of FAK) and coactivation (between Src and FAK). In parallel with these phosphorylation steps, FAK dephosphorylations can be catalysed by phosphatases (Schaller, 2001), among which the tumor suppressor PTEN seems to be the most probable candidate (Gu et al., 1998; Tamura et al., 1998).

In the present paper, we develop a mathematical model for the FAK/Src kinase system in integrin-mediated signaling, based on this sequential scheme. Our aim is to investigate the dynamics of the activation and phosphorylation steps in this enzyme system. Moreover we question a property that has been hypothesized in previous experimental works according to which this system could represent a mechanism for the amplification of integrin-mediated signals (Owen et al., 1999; Ruest et al., 2000). The key idea is that the presence of small amounts of active FAK would increase the quantity of pY397FAK, which would, in turn increase the formation of active FAK. In other words, low amounts of active FAK would switch on an indirect feedback loop that, in the presence of non-phosphorylated FAK and unactive Src, would ultimately drive the system to a state with high levels of active FAK.

The paper is organized as follows. In the next section, we present in detail the mathematical model developed, together with the necessary assumptions we made. Its mathematical expression consists of three coupled non-linear ordinary differential equations, that we study in the next sections. In Section 3, we study analytically and numerically the amplification properties of the model. We show that amplification can indeed occur in certain conditions, and obtain a quantitative condition for this. Section 4 shows that, under constant influx of non-phosphorylated FAK, oscillations may spontaneously appear. Finally, we discuss in Section 5 the biological implications of our results as well as the significance of our model with respect to the corresponding mechanisms *in vivo*.

## 2. The model

Our model is summarized by the biochemical scheme displayed in Fig. 1. We consider the enzymes as

homogeneously distributed and in a single compartment. As a first step, we chose to ignore every detail pertaining to physical segregation of the enzymes inside FAs, or molecular interactions not related to the two kinases considered, leaving further refinements for future works. The present model thus focusses on the dynamics of the FAK/Src enzyme activation system.

The lower part of Fig. 1 concerns Src activation. We note the concentrations of non-phosphorylated (inactive) FAK ( $FAK^*$ ), Y397-phosphorylated FAK ( $pFAK^*$ ), active FAK ( $3pFAK$ ), active Src ( $Src$ ) and inactive Src ( $Src^*$ ) as  $u$ ,  $v$ ,  $w$ ,  $x$  and  $y$ , respectively. To keep the model tractable, we had to make some simplifications regarding the detailed molecular scheme. Firstly, we assume that in comparison with the  $Src$ - $pFAK^*$  complex formation, the conformation change needed to activate  $Src^*$  (and thus to allow  $pFAK^*$  phosphorylation by bound  $Src$ ) can be considered as largely irreversible. Thus the chemical species  $3pFAK$  ( $w$ ) is in fact to be understood as a ( $3pFAK$ - $Src$ ) complex and cannot bind a second  $Src^*$  molecule. Secondly, inasmuch as Src binding to pFAK only involves the formation of a molecular complex, and considering the high affinity of Src for pY397FAK (Pawson et al., 2001), we assume it to be faster than the other (enzyme) reactions of the scheme. This yields an equilibrium assumption for this step

$$K_{act} = \frac{yv}{x}. \quad (1)$$

Eq. (1) is a crude approximation of Src activation, simply ensuring that an increase of  $pFAK^*$  concentration,  $v$ , yields an increase of the Src activation ratio  $x/y$ . Noting  $\sigma_T = x + y$  the (conserved) total Src concentration, we obtain

$$x = \sigma_T \frac{v}{K_{act} + v}. \quad (2)$$

The upper part of Fig. 1 summarizes FAK phosphorylation and reduces to three differential equations. Unphosphorylated

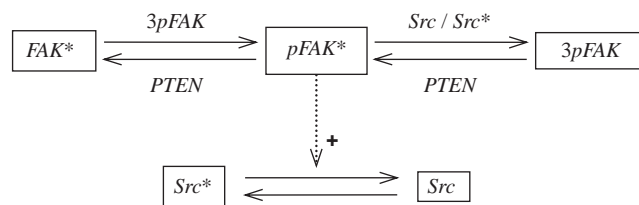


Fig. 1. Scheme of the studied biochemical model. Unphosphorylated inactive FAK,  $FAK^*$ , is phosphorylated on a first tyrosine residue by the fully active FAK,  $3pFAK$ , into a mono-phosphorylated form  $pFAK^*$ . The latter can be turned into the tri-phosphorylated active form,  $3pFAK$ , by the active Src kinase,  $Src$ , as well as, although with lower activity, by the partially inactive Src,  $Src^*$ . PTEN catalyses  $3pFAK$  and  $pFAK^*$  dephosphorylation into  $pFAK^*$  and  $FAK^*$ , respectively. Binding of  $Src^*$  to  $pFAK^*$  stabilizes the former into its fully active form,  $Src$ .

sphorylated FAK ( $u$ ) variations are due to the enzyme activities of  $3pFAK$  and PTEN. We model these variations with two Michaelis–Menten terms

$$\frac{du}{dt} = -k_a w \frac{u}{K_a + u} + V_p \frac{v}{K_p + v}, \quad (3)$$

where  $K_a$  and  $K_p$  are, respectively,  $3pFAK$  and PTEN affinity constants,  $k_a$  is  $3pFAK$  catalytic activity, and  $V_p$  represents PTEN maximum rate.  $pFAK$  dynamics further depend on its activation by  $Src$ . This is a biochemically complex process, which includes double phosphorylation of  $pFAK$ . However, for the seek of simplicity we have chosen here to model it as a Michaelis–Menten term, with  $pFAK$  as the substrate and  $Src$  the enzyme. Furthermore,  $Src^*$  is not totally inactive in vitro, but retains approximately 20% activity with respect to the fully active form (Boerner et al., 1996). However, as compared to its active counterpart, the access of  $Src^*$  to pFAK phosphorylation sites might be different. We chose to lump together the influences of the difference in enzyme activity and accessibility in a unique proportionality parameter,  $\alpha$ . Several reports indicate that in certain cases, unbound Src can phosphorylate FAK without binding to it. For instance, in *src*-transformed cells, Src can phosphorylate Y397F-FAK mutants, which are defective for Src/FAK association (Schaller, 2001; McLean et al., 2000). A low but non-zero value for  $\alpha$  seems thus biologically realistic. In the present work, we use a value of  $\alpha = 0.2$ , but we checked that lower values do not qualitatively change the results presented thereafter. Hence  $pFAK$  activation rate,  $V_{act}$ , is expressed in the present work as

$$V_{act} = k_c \frac{v}{K_m + v} (x + \alpha y),$$

where  $k_c$  and  $K_m$  are active Src catalytic activity and affinity, respectively, and  $\alpha = 0.2$  represents  $Src^*$  residual activity ratio. Combining with Eqs. (1) and (2), one obtains

$$V_{act} = k_c \frac{\sigma_T v}{K_m + v} \left[ \frac{v}{K_{act} + v} (1 - \alpha) + \alpha \right].$$

Finally, we note that experimental evidences (Boerner et al., 1996; Thomas et al., 1998) suggest that  $K_m \simeq K_{act} \equiv K$ , which allows further simplifications for  $V_{act}$

$$V_{act} = k_c \frac{\sigma_T v (\alpha K + v)}{(K + v)^2}. \quad (4)$$

Eq. (4) defines a rate equation that varies from hyperbolic Michaelis–Menten (for  $\alpha \rightarrow 1$ ) to sigmoid cooperative kinetics (for  $\alpha \rightarrow 0$ ). The case  $\alpha = 0.2$  correspond to a mildly cooperative rate. We thus model

*pFAK* dynamics as

$$\frac{dv}{dt} = k_a w \frac{u}{K_a + u} - V_p \frac{v}{K_p + v} - k_c \frac{\sigma_T v (\alpha K + v)}{(K + v)^2} + V_p \frac{w}{K_p + w}. \quad (5)$$

Note that the last term in the right-hand side of Eq. (5) corresponds to *3pFAK* dephosphorylation by PTEN and assumes that PTEN activity and affinity do not change whether the substrate is *pFAK* or *3pFAK*.

In the same way, we model *3pFAK* variations by

$$\frac{dw}{dt} = k_c \frac{\sigma_T v (\alpha K + v)}{(K + v)^2} - V_p \frac{w}{K_p + w}. \quad (6)$$

As a further simplification, we note that PTEN displays a wide range of possible substrates. Actually, in addition to its tyrosine phosphatase activity, PTEN exhibits both serine/threonine and lipid phosphatase activities (Myers et al., 1997, 1998). Such a broad activity spectrum would imply a rather low affinity for the various phosphorylated forms of FAK. We thus assume  $K_p \gg (v, w)$ . Defining  $\eta \equiv V_p/K_p$ , Eqs. (3), (5) and (6) become Eqs. (7)–(9)

$$\frac{du}{dt} = -k_a w \frac{u}{k_a + u} + \eta v, \quad (7)$$

$$\frac{dv}{dt} = k_a w \frac{u}{K_a + u} - \eta(v - w) - k_c \frac{\sigma_T v (\alpha K + v)}{(K + v)^2}, \quad (8)$$

$$\frac{dw}{dt} = k_c \frac{\sigma_T v (\alpha K + v)}{(K + v)^2} - \eta w. \quad (9)$$

Note that we have checked that the assumption of a linear rate for PTEN does not qualitatively change the observed behaviors and dynamics. Our model thus consists of the three ordinary differential equations (ODEs) Eqs. (7)–(9). We non-dimensionalize these equations by rescaling concentrations with  $K$  and time with the inverse of Src catalytic activity,  $1/k_c$ :  $\tilde{u} = u/K$ ,  $\tilde{v} = v/K$ ,  $\tilde{w} = w/K$  and  $\tilde{t} = k_c t$ .

Dropping the tildes for clarity, Eqs. (7)–(9) then read

$$\frac{du}{dt} = -\kappa w \frac{u}{J_a + u} + \lambda v, \quad (10)$$

$$\frac{dv}{dt} = \kappa w \frac{u}{J_a + u} - \lambda(v - w) - \frac{\rho_T v (\alpha + v)}{(1 + v)^2}, \quad (11)$$

$$\frac{dw}{dt} = \frac{\rho_T v (\alpha + v)}{(1 + v)^2} - \lambda w, \quad (12)$$

with the dimensionless parameters  $\kappa = k_a/k_c$ ,  $J_a = K_a/K$ ,  $\lambda = \eta/K$  and  $\rho_T = \sigma_T/K$ .

Variation ranges for some of the parameters can be estimated on the basis of experimental studies. Src affinity and catalytic constants have been estimated with small artificial peptides as substrates to

$K_m \approx K_{act} \equiv K \in [50-100] \mu\text{M}$  and  $k_c \in [30-700] \text{min}^{-1}$  (Boerner et al., 1996; Thomas et al., 1998). *3pFAK* catalytic parameters on similar artificial substrates have also been estimated to  $K_a \approx K$  and  $k_a \approx 1 \text{min}^{-1}$  (Withers et al., 1996).

### 3. Amplification properties

We first notice that Eqs. (10)–(12) conserve the total FAK concentration  $\phi_T = u(t) + v(t) + w(t)$ . The system can thus be reduced to two ODEs

$$\frac{du}{dt} = -\kappa \frac{u(\phi_T - u - v)}{J_a + u} + \lambda v, \quad (13)$$

$$\frac{dv}{dt} = \kappa \frac{u(\phi_T - u - v)}{J_a + u} + \lambda(\phi_T - u - 2v) - \frac{\rho_T v (\alpha + v)}{(1 + v)^2}. \quad (14)$$

A first fixed point,  $\text{FP1}(u_1, v_1)$ , can immediately be found  $(u_1, v_1) = (\phi_T, 0)$ .

FP1 corresponds to a non-amplified state, where all the FAK is found under the non-phosphorylated form. Examination of the phase plane portrait (Fig. 2) reveals the existence of a second fixed point,  $\text{FP2}(u_2, v_2)$ , for some parameter values. This second fixed point corresponds to an amplification state, with  $u_2 < \phi_T$  and non-zero values for  $v_2$  and  $w_2$ . The jacobian matrix,  $\mathbf{J}$ , evaluated at FP1 reads

$$\mathbf{J}(\text{FP1}) = \begin{bmatrix} A & A + \lambda \\ -A - \lambda & -A - 2\lambda - \alpha\rho_T \end{bmatrix},$$

where  $A = \kappa\phi_T/(J_a + \phi_T)$ .  $\mathbf{J}$  eigenvalues,  $\xi_1$  and  $\xi_2$ , can be obtained from the characteristic equation. We find

$$\xi_{1,2} = -1/2\{\alpha\rho_T + 2\lambda \pm \sqrt{\Delta}\}, \quad (15)$$

where  $\Delta = \alpha\rho_T(\alpha\rho_T + 4\lambda + 4A)$ . Studying  $\xi_1$  and  $\xi_2$  sign shows that FP1 is

- (1) a stable node if  $\rho_T < \rho_{Tc}$ ;
- (2) a saddle point for  $\rho_T > \rho_{Tc}$

with

$$\rho_{Tc} = \frac{\lambda^2(J_a/\phi_T + 1)}{\alpha\kappa}. \quad (16)$$

We present bifurcation diagrams for the fraction of non-phosphorylated FAK,  $u/\phi_T$  and that of tri-phosphorylated FAK,  $w/\phi_T$  on Fig. 3. They confirm the occurrence of a transcritical bifurcation at  $\rho = \rho_{Tc}$ . For  $\rho < \rho_{Tc}$ , FP2 is unstable (and yields negative values for  $v$  and  $w$ ) so that the only stable accessible state is FP1, i.e. the system is attracted by the unamplified steady-state. Conversely, when  $\rho > \rho_{Tc}$ , FP1 is unstable while FP2 stable and biologically realistic. The ODE system thus settles onto the amplified state FP2.

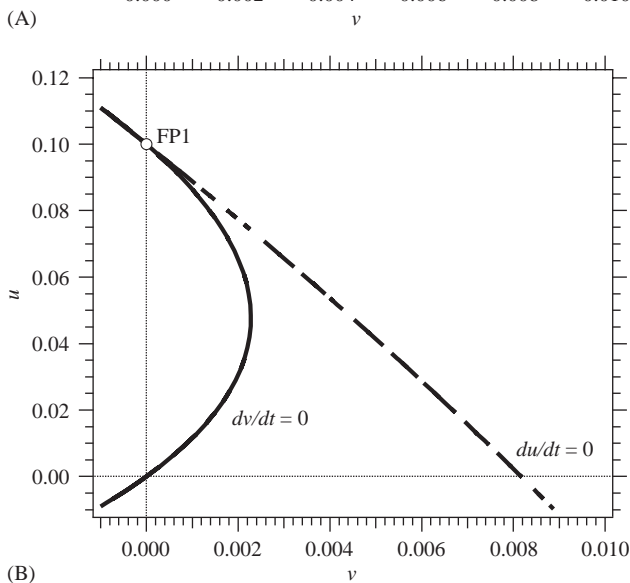
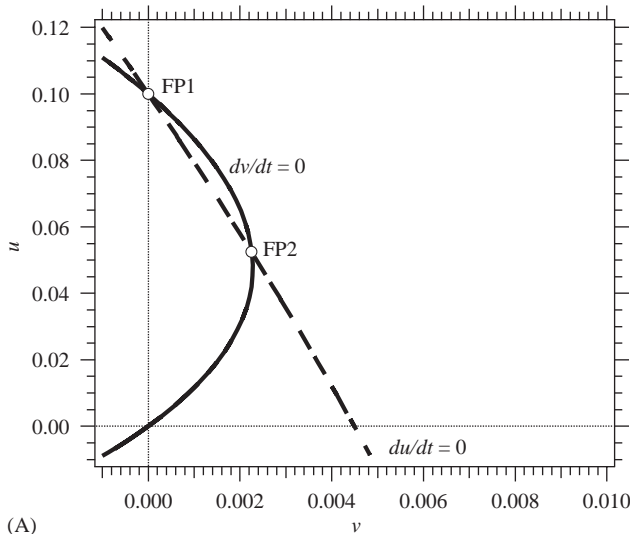


Fig. 2. Phase plane portrait for Eqs. (13) and (14) with (A)  $\rho_T = 1$  or (B)  $\rho_T = 0.5$ .  $\dot{u} = 0$  nullclines are sketched as dashed lines and  $\dot{v} = 0$  nullclines as full ones. The dotted lines mark  $u = 0$  and  $v = 0$ . Other parameters:  $\phi_T = 0.1$ ,  $J_a = 1$ ,  $\lambda = 0.01$ ,  $\kappa = 0.01$  and  $\alpha = 0.2$ .

Hence, analysis of Eqs. (13) and (14) shows that amplification is possible as soon as  $\rho > \rho_{Tc}$ . This amplification condition can be rewritten in terms of the original parameters as

$$\text{Amplification if } \sigma_T > K\eta^2 / (\alpha k_a k_c) (K_a / \phi_T + 1). \quad (17)$$

In other words, the system will display amplification dynamics if the Src concentration is larger than a certain threshold value. We illustrate this property by numerical integrations of Eqs. (13) and (14) (Fig. 4). In these figures, we set the initial conditions to  $v(0) = w(0) = 0$  and (Fig. 4A)  $u(0) = 0.05$  or (Fig. 4B to D)  $u(0) = 0.5$ . At the times indicated by the arrows,  $w$  is increased to 0.01, in order to initiate the amplification mechanism. In Fig. 4A, after  $w$  addition,  $\phi_T = 0.06$ , thus  $\rho_{Tc} = 0.883 > \rho_T$ . Accordingly, after the perturbation,

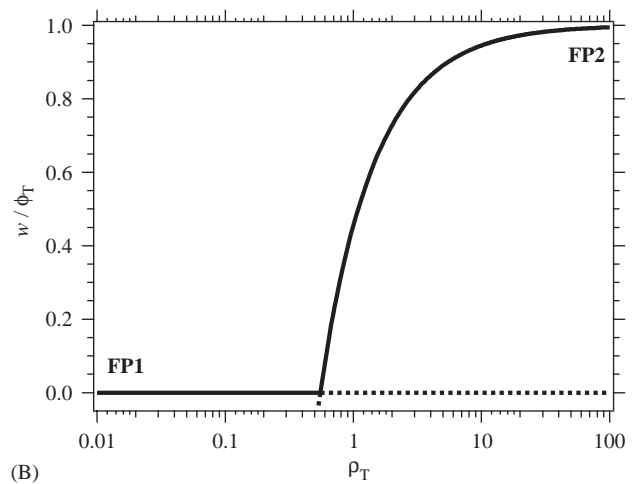
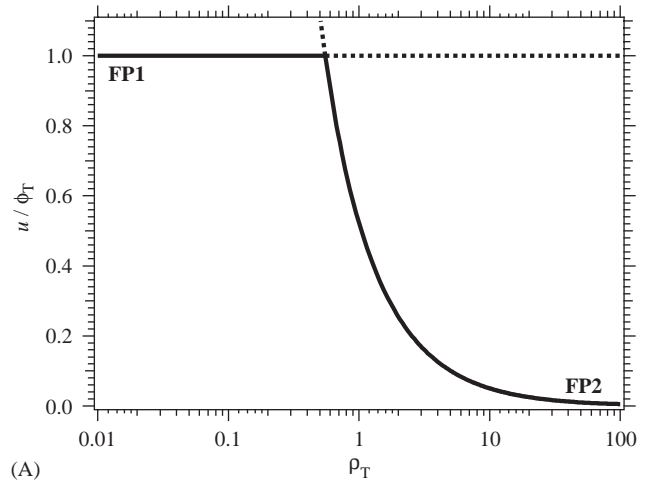


Fig. 3. Bifurcation diagrams for the values of (A) the  $u$ -fraction,  $u/\phi_T$ , or (B)  $w$ -fraction,  $w/\phi_T$ , at the two fixed points, with  $\rho_T$  the control parameter (Eqs. (13) and (14)). Full lines mark stable fixed points, whereas dashed lines represent unstable ones. Parameters are:  $\phi_T = 0.1$ ,  $J_a = 1$ ,  $\lambda = 0.01$ ,  $\kappa = 0.01$  and  $\alpha = 0.2$ .

the systems goes back onto its initial unamplified steady-state. The addition of an active FAK quantity representing 1/6 of the total FAK quantity could not initiate amplification. In Fig. 4B, all parameters have been kept unchanged w.r.t. Fig. 4A, but the initial unphosphorylated FAK quantity is higher, so that  $\rho_{Tc} = 0.148 < \rho_T$ . In this case, the addition of an active FAK amount accounting for 1/51 of the total FAK quantity is sufficient to switch on the amplification mechanism. Thus, this shows that the amplification properties of the system do not really depend on the fraction of active FAK added to initiate the amplification, but on the total FAK quantity (phosphorylated + unphosphorylated forms) at the initiation of the amplification. As a consequence, if active FAK quantity is non-zero, the system can switch to the amplified state through increases of any of the FAK phosphorylation forms ( $u$ ,  $v$  or  $w$ ).

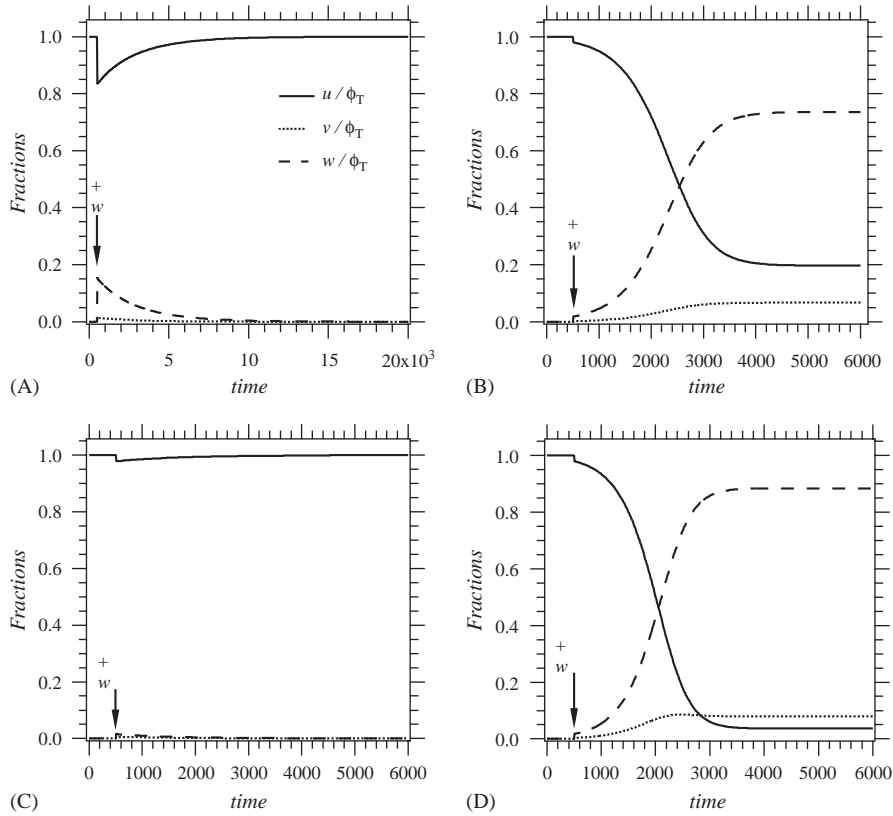


Fig. 4. Numerical solutions of the system Eqs. (13) and (14), illustrating the parameter control of the amplification properties. In each panel, initial conditions are  $v(0) = w(0) = 0$  and (A)  $u(0) = 0.05$  or (B–D)  $u(0) = 0.5$ .  $u$ -,  $v$ - and  $w$ -fractions of the total FAK amount,  $\phi_T$ , are shown as full, dotted and dashed lines, respectively. Amplification is initiated by the addition of a low quantity of active FAK,  $w = 0.01$ , at the times indicated by the arrows. Varied parameters are (A and B)  $\lambda = 0.010$ ,  $\rho_T = 0.500$ ; (C)  $\lambda = 0.010$ ,  $\rho_T = 0.100$  and (D)  $\lambda = 0.002$ ,  $\rho_T = 0.100$ . Other parameters are kept constant:  $J_a = 1$ ,  $\alpha = 0.2$ ,  $\kappa = 0.01$ .

The  $\rho_T$  threshold can also be changed through variations of PTEN activity. Fig. 4C shows numerical solutions obtained in the same conditions as in Fig. 4B apart from the Src total quantity, that has been divided by 5, so that  $\rho_{Tc} = 0.148 > \rho_T$  and we would expect non-amplification property. In agreement with Eq. (16), the system is not amplified after active FAK addition. Finally, in Fig. 4D,  $\lambda$  has been divided by 5, as would be expected if the phosphatase PTEN quantity was decreased by this factor. As predicted by Eq. (16) ( $\rho_{Tc} = 0.006 < \rho_T$ ), amplification is recovered after active FAK addition.

Upon amplification, whether mono-phosphorylated ( $v$ ) or tri-phosphorylated ( $w$ ) forms are preferentially amplified mainly depends on PTEN ( $\lambda$ ) and Src ( $\rho_T$ ) activities. Fig. 5 presents the evolution of the stable fixed point (FP2) with varying  $\lambda/\rho_T$  ratio while keeping  $\lambda^2/\rho_T$  constant.

Whereas the decrease of the  $u$ -fraction hardly depends on  $\lambda/\rho_T$  (Fig. 5), this ratio determines the preferential amplification of  $v$  and  $w$  from  $u$ . Mono-phosphorylated FAK is mostly amplified for high  $\lambda/\rho_T$  ratios, while the active tri-phosphorylated form is prominent for low

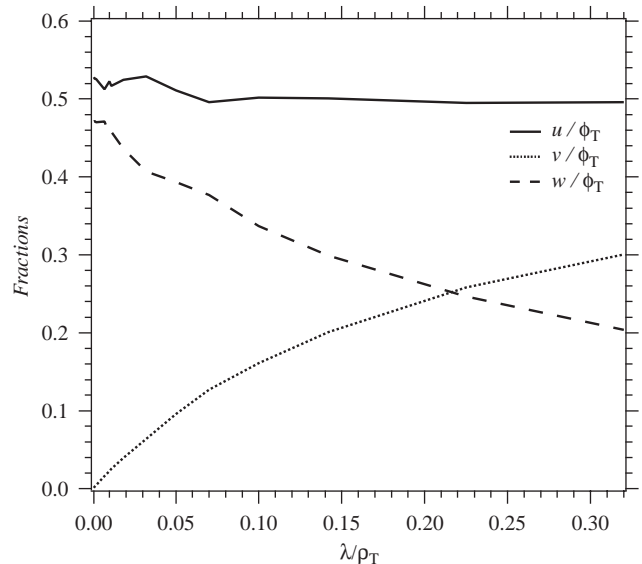


Fig. 5. Evolution of the stable fixed point (FP2) for the values of the fractions of  $u$  (full lines),  $v$  (dotted lines), and  $w$  (dashed lines) at steady-state, with  $\lambda/\rho_T$  the control parameter and  $\lambda^2/\rho_T$  kept constant ( $\lambda^2/\rho_T = 10^{-4}$ ). Parameters are:  $\kappa = 0.01$ ,  $\phi_T = 0.1$ ,  $J_a = 1$  and  $\alpha = 0.2$ .

ratios. Thus the model reflects the intuitive expectation that high PTEN or low Src quantities favor mono-phosphorylated FAK, while low PTEN or high Src quantities yields high amounts of active FAK.

#### 4. Oscillations

To be closer to the in vivo conditions, we now present an “open” version of our model, where total protein concentrations are not conserved. To keep the model as simple as possible, we consider a constant input flow of  $FAK^*$ ,  $I$ , that can be considered as resulting from constant-rate enzyme synthesis by the cell. Similarly,  $pFAK$  and  $3pFAK$  are docking proteins that bind other molecules in the signaling pathway. We assume that the rate at which these complexes form are pseudo-first order in  $pFAK^*$  or  $3pFAK$ , with rate constants  $b$  and  $c$ , respectively. Eqs. (10)–(12) are then modified to Eqs. (18)–(20) (non-dimensionalized version):

$$\frac{du}{dt} = \psi - \kappa w \frac{u}{J_a + u} + \lambda v, \tag{18}$$

$$\frac{dv}{dt} = \kappa w \frac{u}{J_a + u} - \lambda(v - w) - \frac{\rho_T v(\alpha + v)}{(1 + v)^2} - \beta v, \tag{19}$$

$$\frac{dw}{dt} = \frac{\rho_T v(\alpha + v)}{(1 + v)^2} - (\lambda + \gamma)w, \tag{20}$$

where the new dimensionless parameters are:  $\psi = I/(Kk_c)$ ,  $\beta = b/k_c$  and  $\gamma = c/k_c$ . Because of the continuous  $u$  influx, the former point  $FP1(u_1, v_1, w_1) = (\phi_T, 0, 0)$  is not a fixed point of Eqs. (18)–(20). Fixed points  $(u_0, v_0, w_0)$  are solutions of the cubic polynomial

$$v_0^3 + (2 + B/\beta - \psi/\beta)v_0^2 + (1 + \alpha B/\beta - 2\psi/\beta)v_0 - \psi/\beta = 0, \tag{21}$$

where  $B \equiv \rho_T \gamma / (\lambda + \gamma)$ .  $w_0$  and  $u_0$  can then be deduced from  $v_0$

$$w_0 = \frac{\psi - \beta v_0}{\gamma}, \tag{22}$$

$$u_0 = \frac{J_a(\psi + \lambda v_0)}{\kappa w_0 - (\lambda v_0 + \psi)}. \tag{23}$$

We could not find analytical solutions to Eq. (21). Descartes’ rule of signs however indicates that Eq. (21) possesses a unique real positive root. We first present numerical studies of the evolution and stability of this unique fixed point, with  $\rho_T$  the bifurcation parameter (Fig. 6). Here again, amplification occurs for high enough  $\rho_T$  values, for which the fixed point is stable. Note that with the parameter set used in Fig. 6,  $u$  and  $w$  are preferentially amplified. As already mentioned above, other parameters (especially those yielding a

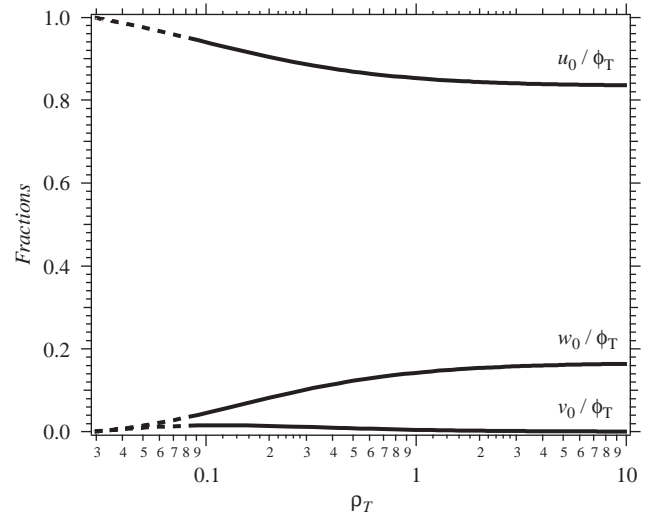


Fig. 6. Bifurcation diagrams for Eqs. (18)–(20) showing the values of the fractions of  $u$ ,  $v$ , and  $w$  at steady-state, with  $\rho_T$  the control parameter. Full lines indicate that the fixed point is stable, whereas dashed lines indicate unstable fixed point. Parameters are:  $\psi = 10^{-4}$ ,  $\beta = \gamma = 0.002$ ,  $\lambda = 0.005$ ,  $\kappa = 0.01$ ,  $J_a = 1$  and  $\alpha = 0.2$ .

higher  $\lambda/\rho_T$  ratio) would lead to a preferential  $v$  amplification.

Biological significance forces  $u_0 > 0$ . In Figs. 6 and 7A, numerical estimations allows to predict the existence of a positive fixed point for  $\rho_T > 0.0295$ . Furthermore, for some  $\rho_T$  value ( $\approx 0.076$  in Figs. 6 and 7A), the fixed point loses its stability through a Hopf bifurcation. The loss of stability of the fixed point is accompanied by simultaneous appearance of a stable limit cycle around it, that drives the system into spontaneous oscillations (Fig. 7B).

We further describe spontaneous oscillations through stability diagrams. Fig. 8 shows the evolution of the Hopf bifurcation and the border representing the fixed point disappearance, when  $\kappa$  and  $\rho_T$  are varied. Also included in this figure is the border indicating the end of the limit cycle (see below). This diagram shows that oscillations spontaneously develop for low  $\kappa$  values and disappear with low  $\rho_T$  values. In other words, oscillations appear when the  $u \rightarrow v$  transformation rate is slower than  $v \rightarrow w$  (i.e. when  $k_a < k_c$  and Src quantity is high enough). This means that oscillations appear when FAK enzyme activity is lower than Src activity. We note that this condition, namely  $k_a < k_c$ , seems to be fulfilled in vivo (see Section 2).

Fig. 9 presents stability diagrams with  $\psi$  and  $\lambda$  the parameters. A first frontier (dashed line) separates the diagram into two zones: a zone where the system displays a fixed point (left-hand side of the frontier) and a zone devoid of biologically realistic fixed point (right-hand side of the frontier). This frontier reflects the condition for positive  $u_0$ . The no-fixed point zone is thus defined by  $\psi > \kappa w_0 - \lambda v_0$ , i.e. corresponds to relatively

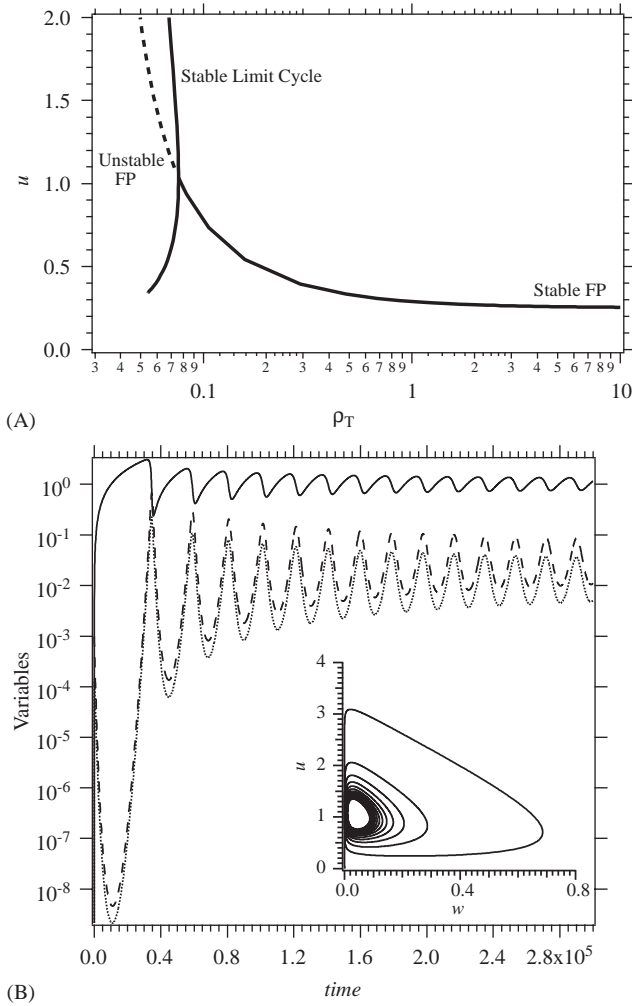


Fig. 7. Hopf bifurcation for Eqs. (18)–(20) with  $\rho_T$  the bifurcation parameter. (A) Plot of the  $u$  values of the fixed point. The dashed line indicates that the fixed point is unstable. Full lines indicate stability of the fixed point or min and max values of the stable limit cycle. (B) Numerical solutions at  $\rho_T = 0.07595$ .  $u$ ,  $v$  and  $w$  time-evolutions are shown as full, dotted and dashed lines, respectively. Initial values were  $u(0) = v(0) = 0$ , and  $w(0) = 0.001$ . The inset shows the corresponding projection of the trajectories in the  $u$ – $w$  phase plane. Other parameters are those of Fig. 6.

large  $\psi$  values. Numerical solutions show that, in this zone,  $\psi \gg \kappa w \frac{u}{J_a + u} + \lambda v$ , so that  $du/dt \approx \psi$  and  $u(t)$  increases linearly. Whatever  $\psi$  value,  $u$  eventually reaches large values such that  $u \gg J_a$  (corresponding to the saturation of  $3pFAK$ ). At this point, the system becomes uncoupled, and Eqs. (18) and (19) reduce to

$$\frac{du}{dt} = \psi, \tag{24}$$

$$\frac{dv}{dt} = \kappa w - \lambda(v - w) - \frac{\rho_T v(\alpha + v)}{(1 + v)^2} - \beta v \tag{25}$$

and  $dw/dt$  is still given by Eq. (20). The ODEs Eqs. (20) and (25) are independent of  $u$ , and possess up to three fixed points:  $FP3(v_3, w_3) = (0, 0)$ ;  $FP4(v_4, w_4)$  and

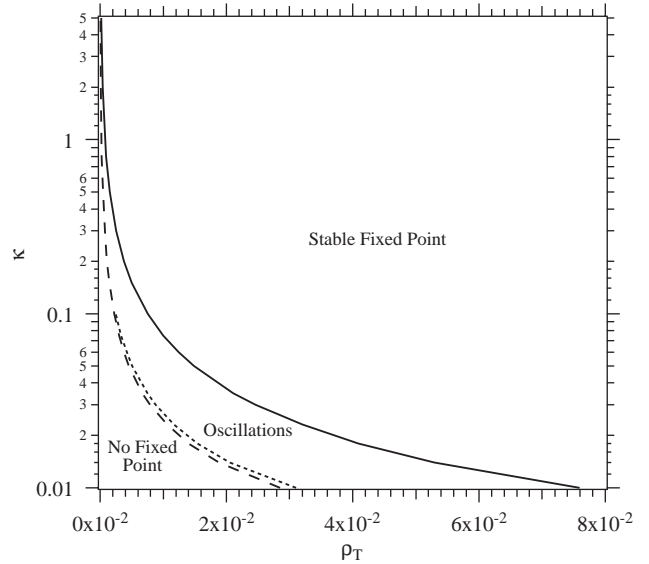


Fig. 8.  $\kappa$ – $\rho_T$  stability diagram for Eqs. (18)–(20). The full line marks the Hopf bifurcation, the dotted line indicates the limit of the limit cycle and the dashed line, the disappearance of the fixed point. Parameters:  $\psi = 10^{-4}$ ,  $J_a = 1$ ,  $\beta = \gamma = 0.002$ ,  $\lambda = 0.005$ ,  $\alpha = 0.2$ .

$FP5(v_5, w_5)$ . The last two fixed points are roots of a second-order polynomial:

$$v_{4,5} = 1/2(C - 2 \pm \sqrt{C^2 - 4C(1 - \alpha)}), \tag{26}$$

$$w_{4,5} = v_{4,5}(\lambda + \beta)/(\kappa - \gamma), \tag{27}$$

$$C = \rho_T(\kappa - \gamma)/[(\lambda + \beta)(\lambda + \gamma)]. \tag{28}$$

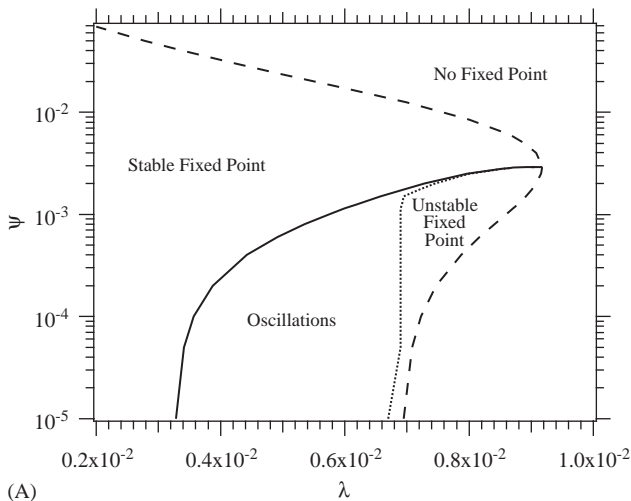
Fig. 10 shows a bifurcation diagram for these fixed points as a function of  $\lambda$ . A transcritical bifurcation between  $FP3$  and  $FP5$  occurs at (for  $\kappa > \gamma$ ):

$$\lambda_1 = \sqrt{\alpha \rho_T(\kappa - \gamma)} - \beta.$$

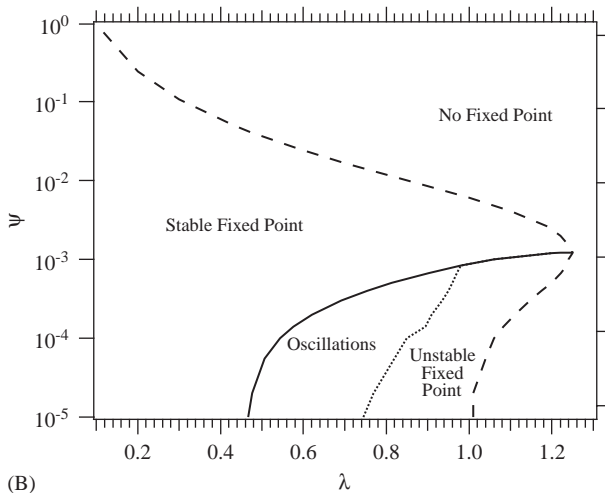
$FP4$  and  $FP5$  then merge and disappear in a saddle-node bifurcation at (for  $\alpha < 0.5$ )

$$\lambda_2 = \sqrt{\frac{\rho_T(\kappa - \gamma)}{4(1 - \alpha)}} - \beta.$$

Actually, we found that  $\lambda_2$  is the “tri-critical” point of Fig. 9, i.e. the intersection of the three borders. Hence, for  $\lambda_1 < \lambda < \lambda_2$ , Eqs. (20), (25) display bistability properties. These properties are also partly shared by the full three-dimensional system Eqs. (18)–(20), as soon as  $3pFAK$  saturation is conserved throughout the dynamics. This condition is guaranteed whenever  $\psi > \kappa w_4 - \lambda v_4$ . We illustrate these properties with numerical solutions of the full three-dimensional system Eqs. (18)–(20) (Fig. 11). In this figure, the three ODEs are integrated in the no-fixed point zone of Fig. 9A ( $\psi = 0.006$ ,  $\lambda = 0.0088$ ) with two different initial conditions. Note that with these parameters,  $\lambda_1 = 6.94 \times 10^{-3}$



(A)



(B)

Fig. 9.  $\psi - \lambda$  stability diagram for Eqs. (18)–(20) with (A)  $\kappa = 0.01$  or (B)  $\kappa = 100$ . Lines are as in Fig. 8. Other parameters are  $J_a = 1$ ,  $\beta = \gamma = 0.002$ ,  $\rho_T = 0.05$ ,  $\alpha = 0.2$ .

and  $\lambda_2 = 9.18 \times 10^{-3}$ , so that  $\lambda$  falls into the bistability region of the reduced system, and  $\kappa w_4 - \lambda v_4 \approx 0.0054$  so that  $3pFAK$  remains saturated. As predicted by Eq. (24),  $u(t)$  rapidly converges to a linear increase (with slope =  $\psi$ ), while  $v$  and  $w$  settle onto their values in FP3 or FP4, depending on the location of the initial conditions with respect to the basins of attraction of the two fixed points. Thus, in the full system,  $u$  increases indefinitely, while  $v$  and  $w$  evolutions are typical of bistable dynamics. In the case  $\lambda > \lambda_2$ , the only stable fixed point of the uncoupled system is FP3, so that the dynamics of the full system consists in a linear increase of  $u$ , while  $v$  and  $w$  vanish. Finally, Fig. 9 shows another zone where the fixed point is still positive (and unstable), but where the stable limit cycle does not exist anymore (labelled “Unstable fixed point” in the figures). The dynamics of the system in this zone are similar to those observed in the no-fixed point area (see below).

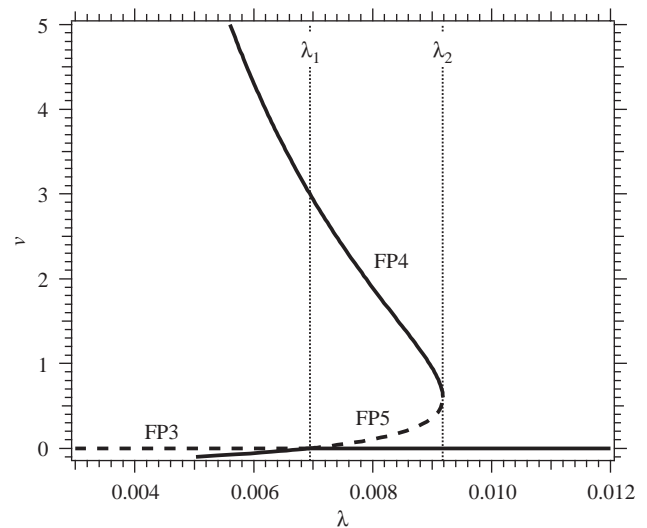


Fig. 10. Bifurcation diagrams for Eqs. (20) and (25) with  $\lambda$  the control parameter. Full lines indicate stable fixed points and dashed lines unstable ones. Fixed point FP3 and FP5 collide in a transcritical bifurcation at  $\lambda = \lambda_1$ , whereas FP4 and FP5 merge and disappear in a saddle-node bifurcation at  $\lambda = \lambda_2$  (see text). Parameters are:  $\kappa = 0.01$ ,  $\beta = \gamma = 0.002$ ,  $\rho_T = 0.05$ ,  $J_a = 1$  and  $\alpha = 0.2$ .

We now turn to the oscillation zone. Fig. 12 presents  $u$ ,  $v$ , and  $w$  time-evolutions during a single oscillation period inside the oscillation zone. We also include the instantaneous rate for  $u \rightarrow v$  transformation by active FAK, i.e.  $\kappa w(t)u(t)/(J_a + u(t))$ . At the beginning of the period,  $v$  and  $w$  are very low. Inasmuch as oscillations arise when  $\kappa$  is low and  $\rho_T$  high enough,  $u \rightarrow v$  is also low, because of the weak  $k_a$  w.r.t.  $k_c$ . Thus  $u$  increases. As  $u$  increases,  $3pFAK$  slowly accumulates. At a point,  $3pFAK$  concentration is high enough to compensate for its low activity and the  $u \rightarrow v$  transformation accelerates. This phenomenon self-amplifies through the mechanisms studied in Section 3, so that  $v$ ,  $w$  and  $u \rightarrow v$  abruptly increase. As a result of this amplification, unphosphorylated FAK\* consumption exceeds its influx by  $\psi$ , and  $u$  decreases. At a point,  $u$  values are of the order of  $J_a$ , and  $3pFAK$  becomes rapidly unsaturated. This causes a rapid decrease of  $3pFAK$  reaction rate ( $u \rightarrow v$ ) even though  $w$  is still increasing. In other words,  $u$  becomes too low to sustain the amplification of  $v$  and  $w$ .  $pFAK^*$  production by  $u \rightarrow v$  starts thus to decline, followed by a rapid decrease of  $v$  and  $w$  due to their consumption by  $\beta$  and  $\gamma$ . Finally,  $v$  and  $w$  are back to low levels, the  $u \rightarrow v$  reaction becomes negligible, allowing  $u$  to increase again, and another cycle begins. Hence, the occurrence of oscillatory behavior in the system is intimately related to its amplification properties.

The oscillation mechanism close to the border indicating the end of the limit cycle is a caricature of this mechanism. During the oscillations,  $u$  increases linearly with a slope equal to  $\psi$ , in a way similar to its

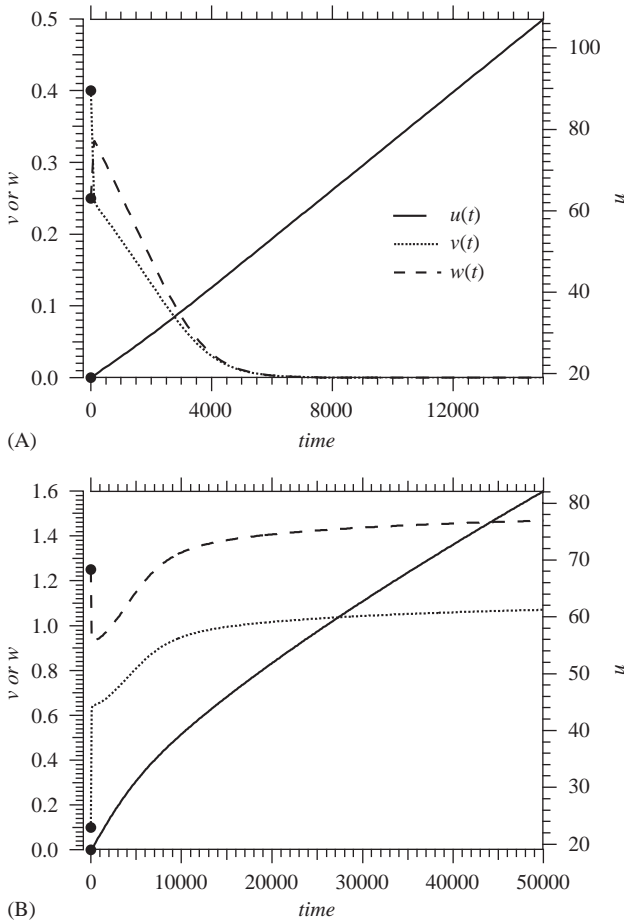


Fig. 11. Uncoupling and bistability in the no-fixed point zone of Fig. 9A. Shown are numerical solutions of Eqs. (18)–(20) (i.e. the full, three-dimensional system) for  $u$  (full lines),  $v$  (dotted lines) or  $w$  (dashed lines) time-evolution, with different initial conditions (indicated with full circles). In (A) initial conditions were  $u(0) = 19$ ,  $v(0) = 0.40$ ,  $w(0) = 0.25$ . In (B)  $u(0) = 19$ ,  $v(0) = 0.10$ ,  $w(0) = 1.25$ . Parameters are:  $\psi = 0.006$ ,  $\lambda = 0.0088$ ,  $\kappa = 0.01$ ,  $\beta = \gamma = 0.002$ ,  $\rho_T = 0.05$ ,  $J_a = 1$  and  $\alpha = 0.2$ .

evolution in the no-fixed point zone (Fig. 13A). During this period,  $v$  and  $w$  remain nearly constant and display very low values. The following amplification-dampening sequence is then very fast as compared to the linear  $u$ -increase phase. This yields typical, “spike-like” oscillations for  $v$  and  $w$  (Fig. 13B). Because of the relatively high PTEN activity close to the border,  $u$  can now increase to high levels before  $w$  reaches values sufficiently high to accelerate the formation of  $pFAK$ . As a result,  $3pFAK$  remains saturated until a short time before the  $u$ -increase phase.

To examine in more details the oscillation mechanism, we define  $\Sigma = u/(J_a + u)$ , the saturation rate of  $3pFAK$ . As  $u \gg J_a$  during most of the oscillatory process,  $\Sigma$  most of the time varies very slowly. Let us treat it as a slowly varying parameter of  $v$  dynamics, Eq. (19). The full system (Eqs. (18)–(20)) is then approximated by Eq. (20)

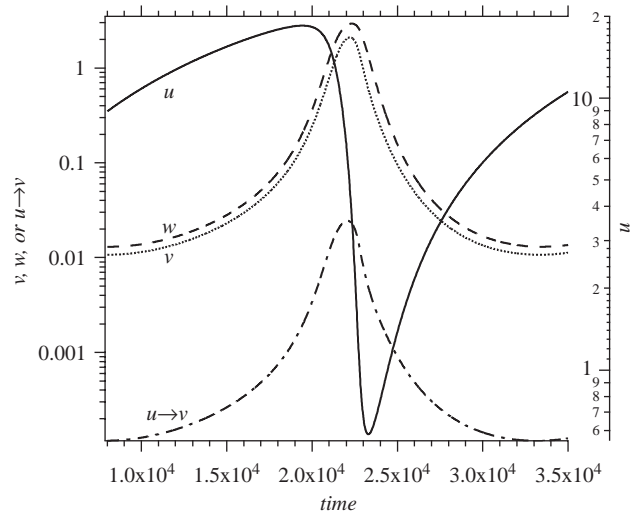


Fig. 12. Numerical solution of Eqs. (18)–(20) during one oscillation period. Presented are  $u$  (full lines),  $v$  (dotted lines),  $w$  (dashed lines) or  $\kappa w u / (J_a + u)$  (mixed dashed-dotted line) time-evolution. Parameters:  $\psi = 0.001$ ,  $\lambda = 0.0065$ ,  $\kappa = 0.01$ ,  $\beta = \gamma = 0.002$ ,  $\rho_T = 0.05$ ,  $J_a = 1$  and  $\alpha = 0.2$ .

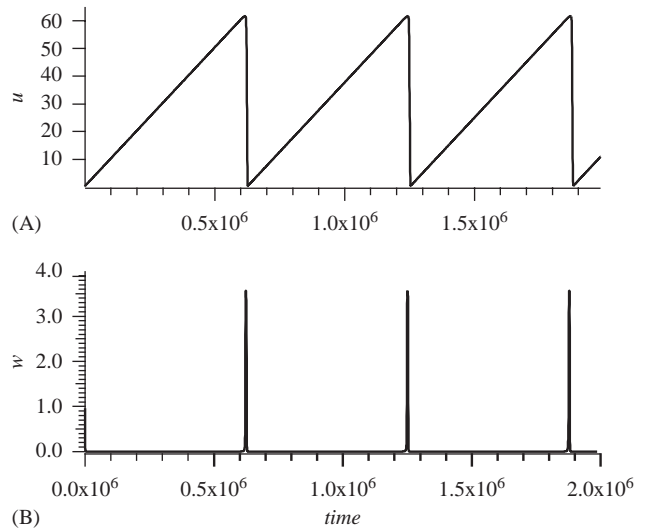


Fig. 13. Oscillations for  $\psi - \lambda$  values close to the end of the limit cycle. Numerical solution of Eqs. (18)–(20) for  $u$  and  $w$  are shown in (A) and (B), respectively. Note that  $v$  time-evolution is similar to that of  $w$  (not shown). Parameters:  $\psi = 0.0001$ ,  $\lambda = 0.0066$ ,  $\kappa = 0.01$ ,  $\beta = \gamma = 0.002$ ,  $\rho_T = 0.05$ ,  $J_a = 1$  and  $\alpha = 0.2$ .

for  $w$  dynamics, and

$$\frac{dv}{dt} = \kappa w \Sigma - \lambda(v - w) - \frac{\rho_T v(\alpha + v)}{(1 + v)^2} - \beta v. \quad (29)$$

As shown in Fig. 14, the bifurcation diagram of the corresponding reduced system (Eqs. (20), (29)) with  $\Sigma$  as bifurcation parameter is bistable, with a low and a high stable branch, both terminated by merging with an intermediate unstable one, via a transcritical and a

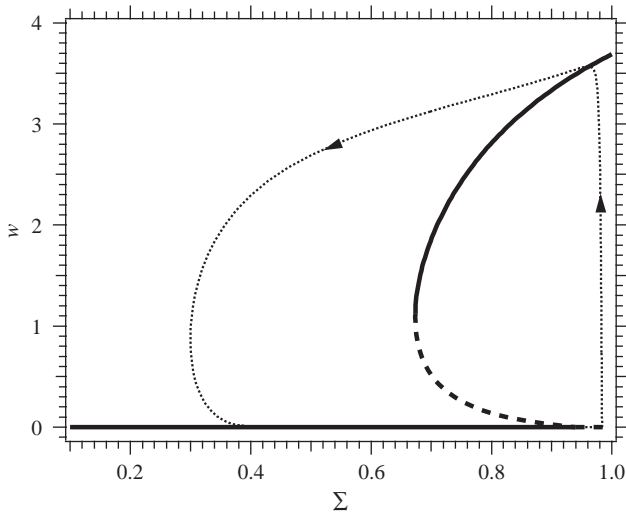


Fig. 14. Bifurcation diagram for the reduced system Eqs. (20) and (29) with  $3pFAK$  saturation rate,  $\Sigma = u/(J_a + u)$ , taken as the bifurcation parameter. Thick full lines represent stable fixed points, and dashed lines unstable ones. Superimposed (thin dotted line) is the evolution of  $w(t)$  as a function of  $u(t)/(J_a + u(t))$  for the full system shown in Fig. 13. The arrows indicate the direction of time passing. Parameters are as in Fig. 13.

saddle-node bifurcation, respectively. Superimposed to the bifurcation diagram of the reduced system, we also show in this figure the evolution of  $w(t)$  as a function of  $u(t)/(J_a + u(t))$  for the full system (Fig. 13A and B). This figure evidences that the behavior of the full system is mostly imposed by the dynamics of the reduced one. In the following, we describe the dynamics of the full system, starting at  $t = 0$  in Fig. 13A and B. When  $u$  is minimal,  $3pFAK$  is unsaturated, so that  $\Sigma$  is lower than the saddle-node bifurcation of the reduced system. Thus the full system settles onto the low branch of the diagram,  $w$  (and  $v$ ) is thus close to zero. As  $u$  increases under the action of  $\psi$ ,  $3pFAK$  saturation slowly increases and the system is driven along the low stable branch. When  $\Sigma$  is greater than its value at the transcritical bifurcation, the low branch becomes unstable, so that the system jumps to the high stable one, resulting in a rapid increase of  $w$  (and  $v$ ) that forms the beginning of the spike. As  $\Sigma$  is very close to 1 at the bifurcation,  $w$  and  $v$  maximum values (on the high stable branch) are very close to  $w_4$  and  $v_4$  (Eqs. (26)–(28)). The resulting acceleration of the  $u \rightarrow v$  rate causes  $u$  and  $\Sigma$  to decrease. At this point, the system follows a trajectory that mimics the high stable branch, but does not exactly settle onto it. This could be due to the fact that, in this part of the oscillation process (i.e. the last moments of  $u$  decrease),  $\Sigma$  variations are not slow anymore. The approximation of the full system by the reduced one is thus largely inaccurate in this part of the dynamics. However, the system eventually reaches low values of  $\Sigma$ , settles onto the only stable branch below the saddle-

node bifurcation (the low one), and another cycle begins.

Hence, the oscillation period in this case depends on the time needed for  $3pFAK$  saturation to be greater than its value at the transcritical bifurcation. Considering that the higher is  $u$ , the slower is  $\Sigma$ -increase w.r.t.  $u$  ( $d\Sigma/du = J_a/(J_a + u)^2$ ), and that  $u(t) \simeq \psi t$  during this phase, this means that the oscillation period can reach large values with low  $\psi$ . For this reason, the limit cycle period close to the border increases dramatically. This has two main consequences. Firstly, the exact determination of this border is a difficult task, so that its representation in the stability diagrams (Fig. 9) lacks accuracy. Secondly, this means that the period varies dramatically, depending on the location in the oscillation zone of the stability diagram. Hence oscillation periods (in dimensionless time) range from 2000 to 10,000 time units close to the Hopf bifurcation to 20,000 to 200,000 time units close to the border indicating the end of the limit cycle. Considering that available estimations of the time-normalization constant  $k_c$  yield  $k_c \approx 100 \text{ min}^{-1}$  (Boerner et al., 1996), the oscillation period would thus range from 20 min to circa 30 h.

Finally, we use the same approach to gain some insights into the ending of the limit cycle. As mentioned above,  $w$  (and  $v$ ) follows the low branch of the bifurcation diagram (Fig. 14) during the phase corresponding to the linear increase of  $u$ . Oscillations then arise if  $v$  and  $w$  both increase sufficiently to switch to the high branch, or if  $dw/dt \gg 0$ . This condition, combined with the fact that  $v \ll \alpha < 1$  on the low branch and Eq. (20) reads

$$v \gg \frac{\lambda + \gamma}{\rho_T \alpha} w.$$

Thus, as  $\lambda$  increases, the switch to the high branch requires increasing values of  $v$  w.r.t.  $w$ . When  $\lambda$  is too high, the switch does not occur, and the oscillations disappear. In this case  $v$  and  $w$  vanish and  $u$  increases indefinitely. This corresponds to the “Unstable fixed point” zone in the stability diagrams (Fig. 9). The oscillations can then be found again if  $\gamma$  is decreased or  $\rho_T$  or  $\alpha$  increased.

## 5. Discussion

In this paper, we have presented a mathematical model for early steps of the signal transduction pathway initiated by integrin receptors during cell adhesion. We focused on the auto- and co-activation scheme made up by the two protein kinases FAK and Src.

We first show that this biochemical organization scheme can indeed amplify incoming signals from bound integrins, in agreement with hypotheses based on experimental studies (Owen et al., 1999; Ruest et al.,

2000), and obtain a quantitative condition for the amplification to be effective (Eq. (17)). Somewhat unexpectedly, this condition shows that the crucial parameter to switch on the amplification mechanism is not the relative quantity of added active  $3pFAK$ , but the total amount of FAK in the system, i.e. the sum of all FAK phosphorylation forms. In a way, the total FAK quantity acts as a critical mass that must be exceeded for active FAK amplification. As a consequence, this means that amplification can occur as a result of an increase in any of the FAK phosphorylation forms, including the non-phosphorylated one.

Secondly, we show that the model may present spontaneous oscillations as a result of the appearance of a Hopf bifurcation. Actually, the underlying oscillation mechanism is closely related to the amplification properties of the system and can be sketched as follows. While the non-phosphorylated form of FAK is injected in the system, its concentration increases up to a value high enough to trigger the amplification mechanism. The concentrations of both phosphorylation forms thus increase, which, in turn, increases the consumption rate of non-phosphorylated FAK that eventually declines down to a value where the amplification is switched off, and another cycle begins.

An important condition for the oscillations to appear in the model is that FAK enzyme activity must be lower than Src activity (i.e.  $\kappa \ll 1$ ). Inasmuch as this condition seems to be fulfilled in vivo (Boerner et al., 1996; Withers et al., 1996), we think that the oscillations of FAK predicted by the model could be biologically realistic. An important consequence of this condition is however that the system dynamics in the oscillatory case are very slow, as can be judged from the oscillation period that ranges from tens of minutes to tens of hours. In fact, periods are so high that, when diffusion is taken into account, the system becomes spatially homogeneous well before the oscillation dynamics take off—at least using biologically realistic diffusion coefficients—(not shown). Now, in our system, the oscillation period is the main characteristic that can be used as a comparison point with experimental data. Kirchner et al. (2003) recently used phosphotyrosine reporters to monitor the dynamic of FAK in focal adhesions. This work shows that FAK reaches its maximal level and return to its initial level in 60 min, although the authors do not mention oscillations in their work because focal adhesions disassembly after one ‘period’. Because we have not taken the influence of FAK phosphorylation on focal adhesions stability into account, the comparison of our results with these experimental measurements is difficult. However, we note that the ‘period’ of the measured FAK time-course is compatible with the oscillations of FAK observed in our model, at least for a domain of the parameter space. The other part of the parameter domain yields oscillations with higher periods

than experimentally observed and whose significance with respect to these experimental results (Kirchner et al., 2003) can be questioned.

As a first hypothesis, we note that time scales in our model primarily depend on the value of Src catalytic constant  $k_c$ . Experimental determinations with artificial small peptides as substrates yielded values around  $100 \text{ min}^{-1}$  (Boerner et al., 1996). In vivo values, with FAK as the substrate, could yield much higher values, so that the oscillation periods predicted by our model would be shorter. Another possibility would be that some other molecular mechanisms, not accounted for in our model, could participate in the generation of FAK oscillations in vivo, in a way that would yield a decrease of the oscillation period. We think for example of concomitant intracellular calcium oscillations, or of the implication of FAK or Src in the turnover (assembling/disassembling) of focal adhesions (Fincham and Frame, 1998; Giannone et al., 2002). In addition, the presently emerging molecular scheme for the FAK/Src activation pathway (Fig. 1) could be an oversimplification of the cell reality. For instance, the autoactivation site of FAK, Y397, could as well be phosphorylated by active Src (Calalb et al., 1995). Furthermore, the implied mechanisms in vivo could be highly variables. For example, artificial suppression of FAK phosphorylation inhibits Src activation in NIH 3T3 cells (Schlaepfer et al., 1998), but not in Swiss 3T3 cells (Rodriguez-Fernandez and Rozengurt, 1996). In confluent NMuMG cells with epithelial phenotype, FAK phosphorylation on tyrosine 397 occurs exclusively in the cytoplasm, and not in FAs, whereas its distribution is just opposite in the same but migrating cells, or in sedentary cells that have been transdifferentiated into the mesenchymal phenotype using TGF- $\beta$ 1 (Nakamura et al., 2001).

Finally, the FAK/Src system is part of a larger signaling network, where many proteins downstream of FAK and Src interact with one or both kinases (Schaller, 2001). FAK itself is even sometimes regarded as an adaptor protein with kinase activity (Schwartz, 2001). Thus it may be that a thorough understanding of the FAK/Src kinase system could necessitate the modelling of the full signaling network. In this work, we assumed to consider both the recruitment and the departure of FAK as constant rates. Future works will have to take the assembly/disassembly of FAs into account as well as the interactions of FAK with integrins and their role in the recruitment of FAK, or other signaling pathways downstream the FAK/Src complex. This is a delicate task as the complexity of the resulting equations often hinders a global understanding of the system. However, this has sometimes proven useful, especially in cases where individual parameters such as enzyme parameters or protein flow rates are well known experimentally. This has for example been the case for modelling of the EGF receptor/MAP kinase

cascade (Schoeberl et al., 2002) or the heregulin induced PI3-K/Akt pathway (Hatakeyama et al., 2003). To our knowledge, the present paper is the first attempt to model the transduction pathways implied in integrin-mediated adhesion. We think that important insights into the dynamics of these signaling cascades will further be provided by more complex mathematical or computational models, but this will need extensive experimental determinations of the in vivo values of the individual parameters needed to quantify these biochemical systems.

## References

- Boerner, R.J., Kassel, D.B., Berker, S.C., Ellis, B., De Lacy, P., Knight, W.B., 1996. Correlation of the phosphorylation states of pp60<sup>c-src</sup> with tyrosine kinase activity: the intramolecular pY530-SH2 complex retains significant activity if Y419 is phosphorylated. *Biochemistry* 95, 9519–9525.
- Bouton, A.H., Riggins, R.B., Bruce-Staskal, P.J., 2001. Functions of the adapter protein Cas: signal convergence and the determination of cellular responses. *Oncogene* 20, 6448–6458.
- Calalb, M.B., Polte, T.R., Hanks, S.K., 1995. Tyrosine phosphorylation of focal adhesion kinase at sites in the catalytic domain regulates kinase activity: a role for src-family kinases. *Mol. Cell Biol.* 15, 954–963.
- Cary, L.A., Guan, J.-L., 1999. Focal adhesion kinase in integrin-mediated signaling. *Front. Biosci.* 4, 102–113.
- Cary, L.A., Han, D.C., Polte, T.R., Janks, S.K., Guan, J.-L., 1998. Identification of p130Cas as a mediator of focal adhesion kinase-promoted cell migration. *J. Cell Biol.* 140, 211–221.
- Chaudhary, A., Brugge, J.S., Cooper, J.A., 2002. Direct phosphorylation of focal adhesion kinase by c-src: evidence using a modified nucleotide pocket kinase and ATP analog. *Biochem. Biophys. Res. Commun.* 294, 293–300.
- Chen, H.-C., Guan, J.-L., 1994. Association of focal adhesion kinase with its potential substrate phosphatidylinositol 3-kinase. *Proc. Natl Acad. Sci. USA* 91, 10148–10152.
- Crowe, D.L., Shuler, C.F., 1999. Regulation of tumor cell invasion by extracellular matrix. *Histol. Histopathol.* 14, 665–671.
- Cukierman, E., Pankov, R., Stevens, D.R., Yamada, K.R., 2001. Taking cell-matrix adhesion to the third dimension. *Science* 294, 1708–1712.
- Damsky, C.H., Ilic, D., 2002. Integrin signaling: it's where the action is. *Curr. Opin. Cell Biol.* 14, 594–602.
- Danen, E.H.J., Yamada, K.M., 2001. Fibronectin, integrins, and growth control. *J. Cell Physiol.* 189, 1–13.
- Fincham, V.J., Frame, M.C., 1998. The catalytic activity of Src is dispensable for translocation to focal adhesions but controls the turnover of these structures during cell motility. *EMBO J.* 17, 81–82.
- Giannone, G., Rondé, P., Gaire, M., Haiech, J., Takeda, K., 2002. Calcium oscillations trigger focal adhesion disassembly in human U87 astrocytoma cells. *J. Biol. Chem.* 277, 26364–26371.
- Gu, J., Tamura, M., Yamada, K.M., 1998. Tumor suppressor PTEN inhibits integrin- and growth factor-mediated mitogen-activated protein (MAP) kinase signaling pathways. *J. Cell Biol.* 143, 1375–1383.
- Hatakeyama, M., Kimura, S., Naka, T., Kawasaki, T., Yumoto, N., Ichikawa, M., Kim, J.-H., Saito, K., Saeki, M., Shirouzu, M., Yokoyama, S., Konagaya, A., 2003. O1\_MRKO1\_MRKA computational model on the modulation of MAPK and Akt pathways in heregulin induced ErbB signaling. *Biochem. J.* 373, 451–463.
- Hynes, R.O., 1999. Cell adhesion, old and new questions. *Trends Biochem. Sci.* 9, M33–M37.
- Ilic, D., Furuta, Y., Kanazawa, S., Takeda, N., Sobue, K., Nakatsuji, N., Nomura, S., Fujimoto, J., Okada, M., Yamamoto, T., 1995. Reduced cell motility and enhanced focal adhesion contact formation in cells from FAK-deficient mice. *Nature* 377, 539–544.
- Katz, B.-Z., Zamir, E., Bershadsky, A., Kam, Z., Yamada, K.M., Geiger, B., 2000. Physical state of the extracellular matrix regulates the structure and molecular composition of cell–matrix interactions. *Mol. Biol. Cell.* 11, 1047–1060.
- Kirchner, J., Kam, Z., Tzur, G., Bershadsky, A.D., Geiger, B., 2003. Live-cell monitoring of tyrosine phosphorylation in focal adhesions following microtubule disruption. *J. Cell Sci.* 116, 975–986.
- Klemke, R.L., Leng, J., Molander, R., Brooks, P.C., Vuori, K., Cheresch, D.A., 1998. CAS/Crk coupling serves as a “molecular switch” for induction of cell migration. *J. Cell Biol.* 140, 961–972.
- LaFlamme, S.E., Auer, K.L., 1996. Integrin signaling. *Cancer Biol.* 7, 111–118.
- Martin, K.H., Slack, J.K., Boerner, S.A., Martin, C.C., Parsons, J.T., 2002. Integrin connection map: to infinity and beyond. *Science* 296, 1652–1653.
- McLean, G.W., Fincham, V.J., Frame, M.C., 2000. v-Src induces tyrosine phosphorylation of focal adhesion kinase independently of tyrosine 397 and formation of a complex with Src. *J. Biol. Chem.* 275, 23333–23339.
- Myers, M.P., Stolarov, J.P., Eng, C., Li, J., Wang, S.I., Wigler, M.H., Parsons, R., Tonks, N.K., 1997. PTEN, the tumor suppressor from human chromosome 10q23, is a dual-specificity phosphatase. *Proc. Natl Acad. Sci. USA* 94, 9052–9057.
- Myers, M.P., Pass, I., Batty, I.H., Van der Kaay, J., Stolarov, J.P., Hemmings, B.A., Wigler, M.H., Downes, C.P., Tonks, N.K., 1998. The lipid phosphatase activity of PTEN is critical for its tumor suppressor function. *Proc. Natl Acad. Sci. USA* 95, 13513–13518.
- Nakamura, K., Yano, H., Schaefer, E., Sabe, H., 2001. Different modes and qualities of tyrosine phosphorylation of FAK and Pyk2 during epithelial-mesenchymal transdifferentiation and cell migration. *Oncogene* 20, 2626–2635.
- Owen, J., Ruest, P.J., Fry, D.W., Hanks, S.K., 1999. Induced focal adhesion kinase (FAK) expression on FAK-null cells enhances cell spreading and migration requiring both auto- and activation loop phosphorylation sites and inhibits adhesion-dependent. *Mol. Cell Biol.* 19, 4806–4818.
- Owens, L.V., Xu, L., Craven, R.J., Dent, G.A., Weiner, T.M., Kornberg, L., Liu, E.T., Cance, W.G., 1995. Overexpression of the focal adhesion kinase (p125FAK) in invasive human tumors. *Cancer Res.* 55, 2752–2755.
- Pawson, T., Gish, G.D., Nash, P., 2001. SH2 domains, interaction modules and cellular wiring. *Trends Cell Biol.* 11, 504–511.
- Reiske, H.R., Kao, S.-C., Cary, L.A., Guan, J.-L., Lai, J.-F., Chen, H.-C., 1999. Requirement of phosphatidylinositol 3-kinase in focal adhesion kinase-promoted cell migration. *J. Biol. Chem.* 274, 12361–12366.
- Reiske, H.R., Zhao, J., Han, D.C., Cooper, L.A., Guan, J.L., 2000. Analysis of FAK-associated signaling pathways in the regulation of cell cycle progression. *FEBS Lett.* 486, 275–280.
- Rodriguez-Fernandez, J.L., Rozengurt, E., 1996. Bombesin, bradykinin, vasopressin, and phorbol esters rapidly and transiently activate Src family tyrosine kinases in Swiss 3T3 cells. *J. Biol. Chem.* 271, 27895–27901.
- Ruest, P.J., Roy, S., Shi, E., Mernaugh, R.L., Hanks, S.K., 2000. Phosphospecific antibodies reveal focal adhesion kinase activation loop phosphorylation in nascent and mature focal adhesions and requirement for the autophosphorylation site. *Cell Growth Differ.* 11, 41–48.
- Ruoslahti, E., 1999. Fibronectin and its integrin receptors in cancer. *Adv. Cancer Res.* 76, 1–20.

- Schaller, M.D., 2001. Biochemical signals and biological responses elicited by the focal adhesion kinase. *Biochim. Biophys. Acta* 1540, 1–21.
- Schaller, M.D., Borgman, C.A., Cobb, B.S., Vines, R.R., Reynolds, A.B., Parsons, J.T., 1992. pp125<sup>FAK</sup>, a structurally distinct protein-tyrosine kinase associated with focal adhesions. *Proc. Natl Acad. Sci. USA* 89, 5192–5196.
- Schaller, M.D., Hilbebrand, J.D., Parsons, J.T., 1999. Complex formation with focal adhesion kinase: a mechanism to regulate activity and subcellular localization of Src kinases. *Mol. Cell. Biol.* 10, 3489–3505.
- Schlaepfer, D.D., Hunter, T., 1997. Focal adhesion kinase overexpression enhances Ras-dependent integrin signaling to ERK2/mitogen-activated protein kinase through interactions with and activation of c-Src. *J. Biol. Chem.* 272, 13189–13195.
- Schlaepfer, D.D., Jones, K.C., Hunter, T., 1998. Multiple Grb2-mediated integrin-stimulated signaling pathways to ERK2/Mitogen-activated protein kinase: summation of both c-src and focal adhesion kinase-initiated tyrosine phosphorylation events. *Mol. Cell. Biol.* 18, 2571–2585.
- Schoeberl, B., Eichler-Jonsson, C., Gilles, E.D., Muller, G., 2002. Computational modeling of the dynamics of the MAP kinase cascade activated by surface and internalized EGF receptors. *Nature Biotechnol.* 20, 370–375.
- Schwartz, M.A., 2001. Integrin signaling revisited. *Trends Cell Biol.* 11, 466–470.
- Slack, J.K., Adams, R.B., Rovin, J.D., Bissonette, E.A., Stoker, C.E., Parson, J.T., 2001. Alterations in the focal adhesion kinase/Src signal transduction pathway correlate with increased migratory capacity of prostate carcinoma cells. *Oncogene* 120, 1152–1163.
- Tamura, M., Gu, J., Matsumoto, K., Aota, S.-I., Parsons, R., Yamada, K.A., 1998. Inhibition of cell migration, spreading and focal adhesions by tumor suppressor PTEN. *Science* 280, 1614–1617.
- Thomas, S.M., Brugge, J.S., 1997. Cellular functions regulated by Src family kinases. *Annu. Rev. Cell Dev. Biol.* 13, 513–609.
- Thomas, J.W., Ellis, B., Boerner, R.J., Knight, W.B., White, G.C., Schaller, M.D., 1998. SH2- and SH3-mediated interactions between focal adhesion kinase and Src. *J. Biol. Chem.* 273, 577–583.
- Vuori, K., Hirai, H., Aizawa, S., Ruoslahti, E., 1996. Induction of p130Cas signaling complex formation upon integrin-mediated cell adhesion: a role for src family kinases. *Mol. Cell. Biol.* 16, 2606–2613.
- Wang, H.-B., Dembo, M., Hanks, S.K., Wang, Y.-L., 2001. Focal adhesion kinase is involved in mechanosensing during fibroblast migration. *Proc. Natl Acad. Sci. USA* 98, 11295–11300.
- Wennerberg, K., Armulik, A., Sakai, T., Karlsson, M., Fässler, R., Schaefer, R.M., Mosher, D.M., Johansson, S., 2000. The cytoplasmic tyrosines of integrin  $\beta 1$  are involved in focal adhesion kinase activation. *Mol. Cell. Biol.* 20, 5758–5765.
- Withers, B.E., Keller, P.R., Fry, D.W., 1996. Expression, purification and characterization of focal adhesion kinase using a baculovirus system. *Protein Expr. Purif.* 7, 12–18.
- Young, M.A., Gonfloni, S., Superti-Furga, G., Roux, B., Kuriyan, J., 2001. Dynamic coupling between the SH2 and SH3 domains of c-Src and Hck underlies their inactivation by C-terminal tyrosine phosphorylation. *Cell* 105, 115–126.